Assessing the potential of SeaWiFS and MODIS for estimating chlorophyll concentration in turbid productive waters using red and near-infrared bands

Giorgio Dall'Olmo[a,b,*], Anatoly A. Gitelson[a,b], Donald C. Rundquist[a,b], Bryan Leavitt[a], Tadd Barrow[b], John C. Holz[b]

[a]Center for Advanced Land Management Information Technologies, 102 Nebraska Hall, University of Nebraska–Lincoln, Lincoln, NE 68588-0517, USA
[b]School of Natural Resources, University of Nebraska–Lincoln, Lincoln, NE 68583, USA

Abstract

Bio-optical algorithms for remote estimation of chlorophyll-a concentration (*Chl*) in case-1 waters exploit the upwelling radiation in the blue and green spectral regions. In turbid productive waters other constituents, that vary independently of *Chl*, absorb and scatter light in these spectral regions. As a consequence, the accurate estimation of *Chl* in turbid productive waters has so far not been feasible from satellite sensors. The main purpose of this study was to evaluate the extent to which near-infrared (NIR) to red reflectance ratios could be applied to the Sea Wide Field-of-View Sensor (SeaWiFS) and the Moderate Imaging Spectrometer (MODIS) to estimate *Chl* in productive turbid waters. To achieve this objective, remote-sensing reflectance spectra and relevant water constituents were collected in 251 stations over lakes and reservoirs with a wide variability in optical parameters (i.e. $4 \leq Chl \leq 240$ mg m^{-3}; $18 \leq$ Secchi disk depth ≤ 308 cm). SeaWiFS and MODIS NIR and red reflectances were simulated by using the in-situ hyperspectral data. The proposed algorithms predicted *Chl* with a relative random uncertainty of approximately 28% (average bias between -1% and -4%). The effects of reflectance uncertainties on the predicted *Chl* were also analyzed. It was found that, for realistic ranges of R_{rs} uncertainties, *Chl* could be estimated with a precision better than 40% and an accuracy better than $\pm 35\%$. These findings imply that, provided that an atmospheric correction scheme specific for the red-NIR spectral region is available, the extensive database of SeaWiFS and MODIS images could be used to quantitatively monitor *Chl* in turbid productive waters.
© 2005 Elsevier Inc. All rights reserved.

Keywords: Chlorophyll; Turbid productive waters; SeaWiFS; MODIS; Uncertainty; Near-infrared; Red

1. Introduction

Turbid productive waters constitute less than 10% of the world surface waters, and yet they represent the majority of the aquatic ecosystems with which the human population interacts. It is therefore of interest to quantitatively monitor their spatio–temporal dynamics in order to predict ecolog-ical changes and the consequences of these changes on human activities. Bio-optical algorithms are devised to relate the electromagnetic energy reflected in the upward direction to the concentrations of the constituents dissolved and suspended in the water column. Among these, the concentration of chlorophyll-a (*Chl*) is one of the most important since it is used to estimate the primary produc-tivity of water ecosystems.

The Sea-viewing Wide Field-of-view Sensor (SeaWiFS) and Moderate Resolution Imaging Spectrometer (MODIS) have been collecting ocean color data since September 1997 and January 2000, respectively, providing an extensive database of images to the scientific community. All opera-

tional *Chl* algorithms exploit the upwelling radiation in the blue and green spectral region (e.g. Darecki & Stramski, 2004; O'Reilly et al., 1998). However, the hypotheses upon which such algorithms are based break down in turbid productive waters because of the presence of other constituents (e.g. chromophoric dissolved organic matter, CDOM) that do not co-vary with *Chl*. Most importantly, because of the high values of the total absorption coefficient (*a*), the signal upwelling in the blue spectral region is often too low (comparable to, or lower than the signal in the near-infrared, e.g. Gons et al., 2000; Lee et al., 1994), thus reducing the sensitivity of these algorithms. As a consequence, *Chl* estimation is affected by large uncertainties. For instance, Darecki and Stramski (2004) applied the MODIS case-2 water *Chl* algorithm (Carder et al., 1999) to estimate *Chl* in the Baltic Sea and obtained a large bias (∼30%) and a large random uncertainty (>100%), even after a regionalization of the algorithm.

On the other hand, authors working with turbid productive inland and coastal waters have focused their attention on the red and near-infrared (NIR) regions of the electromagnetic spectrum, where the absorption by CDOM and non-algal suspended particles is generally negligible (Dall'Olmo et al., 2003; Dekker, 1993; Gitelson & Kondratyev, 1991; Gons, 1999; Gons et al., 2000; Gons et al., 2002; Ruddick et al., 2001). By exploiting the radiation reflected around 700 nm, accurate estimates of *Chl* were possible over a wide range of optical parameters (e.g. Dall'Olmo & Gitelson, 2005; Gons et al., 2000). To date however, the only space-borne ocean color sensor equipped with a channel around 700 nm is the Medium Resolution Imaging Spectrometer (MERIS); the Global Imager (GLI) also measured the upward radiation in such spectral region, but it stopped sending data in October 2003.

Other remote-sensing algorithms have been proposed for coastal waters to attempt to account for the presence of constituents different from *Chl*. These algorithms include, among others, matrix inversion (Hoge & Lyon, 1996), spectrum matching techniques (Garver & Siegel, 1997) and neural network modeling (Schiller & Doerffer, 1999). However, to the authors' knowledge, no technique has shown satisfying results in estimating *Chl* in the range 10–100 mg m^{-3} using SeaWiFS and MODIS data. Indeed, also due to the lack of an operational atmospheric correction scheme for turbid waters, no operational product from SeaWiFS and MODIS is available for estimating *Chl* in turbid productive waters.

Recently, Dall'Olmo and Gitelson (2005) presented a three-band reflectance algorithm for estimating *Chl* in turbid productive waters. This algorithm uses remote-sensing reflectances in the red and NIR spectral region and a special case of it is the simpler NIR-to-red reflectance ratio, which can be analytically related to the absorption by *Chl* in the red channel by assuming that: 1) the total back-scattering coefficient (b_b) and the f/Q factor are approximately equal in the red and NIR bands (*f* is the proportionality factor that

relates the below-water irradiance reflectance to b_b/a and Q is the ratio of the below-water upward irradiance to the below-water upward radiance); 2) the absorption by constituents different from *Chl* and pure water is negligible in the red and NIR bands (Dall'Olmo & Gitelson, 2005; Lyon et al., 2004; Ruddick et al., 2001).

Furthermore, it was found that NIR-to-red reflectance ratios with the numerator located around 750 nm could accurately estimate *Chl* (Dall'Olmo & Gitelson, 2005; Ruddick et al., 2001; Yacobi et al., 1995). Several ocean color sensors are provided with channels in this spectral region (IOCCG Report Number 1, 1998) that, over clear waters, are used to quantify the atmospheric effect (Gordon & Wang, 1994). In turbid waters, however, such a methodology fails because of non-zero water-leaving radiances in the NIR (e.g. Ruddick et al., 2000). Assuming the availability of an atmospheric correction scheme providing water-leaving radiances in the red and NIR, the above algorithm may be used to exploit SeaWiFS and MODIS for the quantitative monitoring of turbid productive waters.

The main objective of this study is to assess the extent to which SeaWiFS and MODIS can be exploited to monitor *Chl* in turbid productive waters. Specific objectives include: (1) the calibration and validation of NIR-to-red ratios using reflectance in simulated SeaWiFS and MODIS channels; and (2) the analysis of the effects of random and systematic uncertainties in R_{rs} on the derived Chl. It is shown that, provided an appropriate atmospheric correction scheme is available, the use of NIR-to-red reflectance ratios is a reliable alternative for estimating *Chl* in turbid productive waters using SeaWiFS and MODIS data.

2. Methodology

2.1. Study area

Two types of water bodies located in Eastern Nebraska (USA) were sampled: sand pit lakes (Fremont State Lakes and Ginger Cove) and reservoirs (Glen Cunningham and Branched Oak). Data were collected during 41 field campaigns from June to October 2001, from May to October 2002, and from April to October 2003. Thus, in addition to the data that were previously published (Dall'Olmo & Gitelson, 2005; Dall'Olmo et al., 2003), 136 stations collected during 2003 were added to the current study, raising the total number of stations to 251.

2.2. Field measurements

Nadir water-leaving remote-sensing reflectance [$R_{rs}(\lambda)$, sr^{-1}] was measured on the sunny side of a small (about 5 m long) boat using two inter-calibrated Ocean Optics USB2000 radiometers. Data were collected in the 400–900 nm range with a sampling interval of 0.3 nm and a spectral resolution of 1.5 nm. Radiometer #1, equipped with

a 25° field-of-view optical fiber was pointed downward to measure the below-surface upward radiance (expressed in digital numbers as DN_{Lu}). The tip of the optical fiber was kept just below the water surface (~ 5 cm), in the nadir direction. Radiometer #2, equipped with an optical fiber and a cosine collector, was pointed upward to simultaneously measure the above-surface downward irradiance (expressed in digital numbers as DN_{Ed}). $R_{rs}(\lambda)$ was computed as (Dall'Olmo & Gitelson, 2005):

$$R_{rs}(\lambda) = \frac{t}{n^2} \frac{DN_{Lu}(\lambda)}{DN_{Ed}(\lambda)} \frac{DN_{Ed,ref}(\lambda)}{DN_{Lu,ref}(\lambda)} \frac{\rho_{ref}(\lambda)}{\pi} F_i(\lambda)$$

where $DN_{Lu,ref}$ and $DN_{Ed,ref}$ are the digital numbers recorded by the downward and upward-looking radiometers, respectively, while the downward-looking instrument viewed a white Spectralon panel; $\rho_{ref}(\lambda)$ is the irradiance reflectance of the Spectralon panel; λ is the wavelength; t is the radiance transmittance from water to air (0.98), n is the refractive index of water (1.33), and $F_i(\lambda)$ is the spectral immersion factor (Ohde & Siegel, 2003; Quan & Fry, 1995). More details about the measurement setup and the derivation of the R_{rs} equation can be found in Dall'Olmo and Gitelson (2005). Note that the Spectralon panel was considered a Lambertian surface. In reality, deviations of up to ±5% from this ideal behavior should be expected for solar zenith angles ranging from 20° to 55° (as in this study) (Sandmeier et al., 1998). Such small deviations however are compensated by reflectance ratios and therefore they are considered negligible in the following analysis. At each station we collected six R_{rs} spectra each averaging 15 consecutive scans. Also, at each station, we measured Secchi disk depth (cm) and nephelometric turbidity (NTU) using a portable Hach 2100 turbidimeter. Surface water samples (~ 0.5 m) were collected for laboratory analyses.

2.3. Laboratory measurements

Chlorophyll-a from algae concentrated on Whatman GF/F filters was extracted in hot ethanol, and its concentration was quantified fluorometrically (Turner Design 10-AU) (Welschmeyer, 1994). The concentrations of total (TSS), organic (OSS), and inorganic suspended solids (ISS) were determined gravimetrically (American Public Health Association et al., 1989). Spectrophotometric measurements were acquired in 2002 and 2003 to determine the absorption coefficients of total and algal particles as well as CDOM (details about these methods have already been published in Dall'Olmo & Gitelson, 2005).

2.4. R_{rs} data preprocessing

The six R_{rs} spectra collected at each station were smoothed (to remove high frequency noise) using a moving average (window size of 5 nm), linearly interpolated every

nanometer and the mean spectra were computed for further analysis. At wavelengths longer than 750 nm, the absorption coefficient of pure water increases drastically in coincidence with the spectral region where the sensitivity of the radiometer used decreases. When either the downward irradiance was low (e.g. overcast sky), or the upward radiance was low (e.g. clear waters), the dark current recorded by the radiometer in this spectral range was comparable to, or higher than, the signal DN_{Lu} and, as a consequence, the R_{rs} spectra exhibited noisy patterns at $\lambda > 750$ nm. Specifically, an increase in R_{rs} at wavelengths longer than 814 nm appeared in noisy spectra (Fig. 1, thick line), while non-noisy R_{rs} spectra mimicked the spectral shape of the inverse of the absorption coefficient of pure water (Fig. 1, thin line). A method to discard these noisy R_{rs} spectra was therefore devised based on the local minimum in water absorption at ~ 814 nm that generates a corresponding local reflectance maximum (Fig. 1). All R_{rs} spectra (19 out of the initial 270) for which $R_{rs}(835) > R_{rs}(814)$ were discarded.

To simulate the $R_{rs}(\lambda_i)$ signals that would be recorded by satellite sensor channels centered at wavelength λ_i, weighted averages of each R_{rs} spectrum were calculated by using as weights the spectral band responses $[SRB(\lambda)]$ of Sea-WiFS (http://oceancolor.gsfc.nasa.gov/DOCS/RSR/SeaWiFS_RSRs.txt) and MODIS Terra (ftp://ftp.mcst.ssai.biz/pub/permanent/MCST/PFM_L1B_LUT_4-30-99/):

$$R_{rs}(\lambda_i) = \frac{\sum_\lambda R_{rs}(\lambda) SBR(\lambda)}{\sum_\lambda SBR(\lambda)}$$

Finally, using the simulated sensor bands, NIR-to-red reflectance ratios were computed (Table 1).
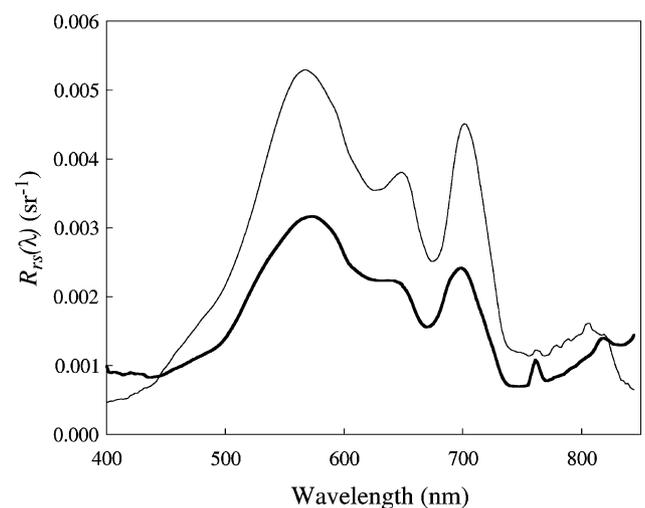

Fig. 1. Example of noisy (thick line) and non-noisy (thin line) R_{rs} spectra. The non-noisy spectrum exhibits a local maximum around 814 nm due to the local minimum in water absorption. For $\lambda > 814$ nm R_{rs} decreases in the non-noisy spectrum due to the increase in water absorption. In contrast, the noisy spectrum is characterized by a general increase in R_{rs} towards longer wavelengths.

Table 1
Algorithms proposed in this study

Sensor	Algorithm	Abbreviation
SeaWiFS	$R_{rs}(765)/R_{rs}(670)$	SeaWiFS(670,765)
MODIS	$R_{rs}(748)/R_{rs}(667)$	MODIS(667,748)
	$R_{rs}(748)/R_{rs}(678)$	MODIS(678,748)

The numbers in parentheses indicate the centers of the bands used in the algorithms. The abbreviations that are used throughout the text are also reported.

2.5. Calibration and validation

The data set was divided into calibration (stations collected in 2003, $N=136$) and a validation (stations collected in 2001 and 2002, $N=115$) subsets. Using the calibration subset, the nonlinear least-squares best fit functions between Chl and each of the algorithms presented in Table 1 were calculated. The accuracy of Chl prediction by each algorithm was then assessed by comparing the predicted Chl values with those measured analytically in the validation data set. This comparison was quantified by means of the percent difference between Chl predicted and Chl measured analytically ($Chl_{observed}$):

$$\varepsilon_i = \frac{Chl_{predicted,i} - Chl_{observed,i}}{Chl_{observed,i}} 100. \quad (1)$$

To exclude outliers, all stations for which $\varepsilon_i > 2s(\varepsilon)$ were removed, where $s(\varepsilon)$ is the experimental standard deviation of ε_i (Zibordi et al., 2004). The average relative bias in Chl prediction, was calculated as the average value of ε_i', $\overline{\varepsilon}'$, where the prime indicates that outliers had been removed. To estimate the relative random uncertainty of Chl prediction, we calculated $s(\varepsilon')$, the experimental standard deviation of ε_i'.

2.6. Random uncertainties

Random uncertainties are related to the precision of a measurement and they can usually be reduced by averaging a large number of measurements (BIPM & ISO, 1995). In the case of a satellite system (space-borne sensor+atmospheric correction scheme+bio-optical algorithm), the overall relative random uncertainty in Chl prediction can be approximated as (Gordon, 1990):

$$\left[\frac{s(Chl)}{Chl}\right]_{system} = \sqrt{\left[\frac{s(Chl)}{Chl}\right]_{bio}^2 + \left[\frac{s(Chl)}{Chl}\right]_{sens}^2} \quad (2)$$

where $[s(Chl)/Chl]_{bio}=s(\varepsilon)$ is the relative random uncertainty in Chl due to the variability in bio-optical parameters (e.g. specific absorption coefficient) that is not accounted for by the bio-optical algorithm; $[s(Chl)/Chl]_{sens}$ is the relative random uncertainty in Chl due to the propagation of the radiometric noise of the sensor through the atmospheric correction scheme and the bio-optical algorithm.

Table 2
Noise-equivalent remote-sensing reflectances [$NE\Delta R_{rs}(\lambda_i)$] computed for red and NIR spectral channels of SeaWiFS and Terra-MODIS

Sensor	λ_i	$E(\lambda_i)$ (W m^{-2} μm^{-1})	$NE\Delta L(\lambda_i)$ (W m^{-2} sr^{-1} μm^{-1})	$NE\Delta R_{rs}(\lambda_i)$ ($10^{-5} \times$ sr^{-1})
SeaWiFS	670	604	0.031	5.1
	765	449	0.019	4.2
MODIS	667	609	0.0073	1.2
	678	597	0.0064	1.1
	748	522	0.0078	1.5

$E(\lambda_i)$ are the above-water downward irradiances (weighted by the spectral band response of the sensor channel centered at λ_i) that were computed for a worst-case atmospheric scenario using the atmospheric radiative transfer code 6S (see text for details).
$NE\Delta L(\lambda_i)$ are the noise-equivalent radiances.

Considering the random uncertainties in $R_{rs}(\lambda)$ to be small, $[s(Chl)/Chl]_{sens}$ can be calculated using the standard law of propagation of uncertainty (BIPM & ISO, 1995):

$$\left[\frac{s(Chl)}{Chl}\right]_{sens} = \frac{1}{Chl}\left\{\sum_{i=1}^{B}\left[\frac{\partial Chl}{\partial R_{rs}(\lambda_i)}s[R_{rs}(\lambda_i)]_{sens}\right]^2 \right.$$
$$+ 2\sum_{i=1}^{B-1}\sum_{j=i+1}^{B}\left[\frac{\partial Chl}{\partial R_{rs}(\lambda_i)}\frac{\partial Chl}{\partial R_{rs}(\lambda_j)}\right.$$
$$\left.\left.\times s^2[R_{rs}(\lambda_i)]_{sens}r(\lambda_i,\lambda_j)\right]\right\}^{0.5} \quad (3)$$

where B is the number of bands used in the bio-optical algorithm, λ_i is the band center of the channel used; $s[R_{rs}(\lambda_i)]_{sens}$ are the random uncertainties associated with $R_{rs}(\lambda_i)$ due to the radiometric noise of the sensor; $r(\lambda_i, \lambda_j)$ is the correlation coefficient between these uncertainties in bands λ_i and λ_j. In Eq. (3) the first term inside the curly parentheses represents the variance in Chl due to uncorrelated R_{rs} uncertainties, while the second term accounts for the correlations among the R_{rs} uncertainties.

Operational atmospheric correction procedures specific for calculating water-leaving radiances in the red-NIR spectral region over turbid waters have, up to now, not been developed for SeaWiFS and MODIS. Thus, an arbitrary decision was made in order to quantify the magnitude of $s[R_{rs}(\lambda_i)]_{sens}$: this uncertainty was expressed as a multiple (g_r) of the noise-equivalent remote-sensing

Table 3
Median Chl and corresponding simulated median SeaWiFS and MODIS remote-sensing reflectances (in units of per steradian) for selected red and NIR channels (indicated by the central wavelength of the channel in nanometers)

Chl (mg m^{-3})	SeaWiFS		MODIS			N
	670	765	667	678	748	
9.8	0.00320	0.00069	0.00322	0.00303	0.00064	19
19.6	0.00562	0.00190	0.00568	0.00527	0.00181	32
45.9	0.00506	0.00290	0.00515	0.00476	0.00266	6
103.5	0.00337	0.00256	0.00335	0.00316	0.00253	4

N is the number of stations used to compute the median.

Table 4
Models that were fitted to each of the algorithms presented in Table 1. Parameters (standard errors), standard errors of estimate and determination coefficients are also reported

Algorithm (I)	Model fitted	a (se)	b (se)	STE (mg m^{-3})	r^2
SeaWiFS(670, 765)	$Chl = 10^{[a + b \times \log_{10}(I)]}$	2.055 (0.011)	1.51 (0.05)	12.9	0.86
MODIS(667, 748)	$Chl = 10^{[a + b \times \log_{10}(I)]}$	2.048 (0.009)	1.38 (0.03)	11.0	0.90
MODIS(678, 748)	$Chl = 10^{[a + b \times \log_{10}(I)]}$	2.046 (0.012)	1.49 (0.05)	13.5	0.85

All parameters are statistically significant ($p < 0.001$). The number of samples was 136.

Table 5
Descriptive statistics of the ancillary data used. TSS, VSS and ISS are the concentration of total, organic and inorganic suspended solids, respectively; $a_{CDOM}(440)$ and $a_{det}(440)$ are the absorption coefficients measured at 440 nm of CDOM and non-algal suspended particles, respectively

	Average	St. dev.	Min	Max	N
Chl (mg m^{-3})	38.5	39.3	4.0	236.5	270
Secchi disk depth (cm)	86	61	18	308	264
Turbidity (NTU)	16.2	13.8	1.3	78.0	263
TSS (mg L^{-1})	17.5	19.8	0.2	213.5	260
VSS (mg L^{-1})	10.8	14.3	0.2	213.5	260
ISS (mg L^{-1})	6.7	12.0	<0.1	139.8	260
$a_{CDOM}(440)$ (m^{-1})	1.09	0.95	0.02	4.41	226
$a_{det}(440)$ (m^{-1})	1.52	1.35	0.33	6.69	206

N is the number of samples.

reflectance (measured just above the water) in the NIR band around 750 nm, NEΔR_{rs}(NIR):

$$s[R_{rs}(\lambda_i)]_{sens} = g_r NE\Delta R_{rs}(NIR) \tag{4}$$

This convention will eventually enable us to compare the results of the uncertainty analysis obtained for the two different sensors. The R_{rs} random uncertainties associated with each spectral band used in the bio-optical model were first assumed to be negatively correlated, i.e. $r(\lambda_i, \lambda_j) = -1$ in Eq. (3), and then to be positively correlated, i.e. $r(\lambda_i, \lambda_j) = 1$. In this way, a worst ($r = -1$) and best ($r = 1$) case scenarios, respectively, were considered.

The NE$\Delta R_{rs}(\lambda_i)$ was computed as:

$$NE\Delta R_{rs}(\lambda_i) = \frac{NE\Delta L(\lambda_i)}{E(\lambda_i)} \tag{5}$$

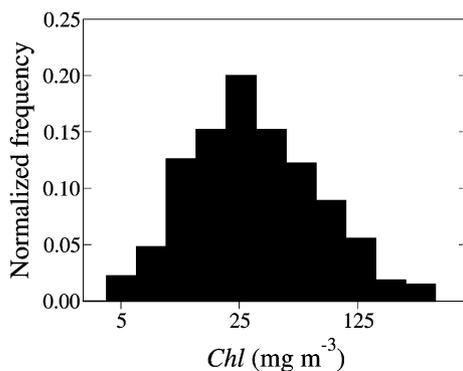where NE$\Delta L(\lambda_i)$ is the noise-equivalent radiance of the sensor channel centered at λ_i; $E(\lambda_i)$ is the downward solar irradiance just above the water surface and weighted by the spectral response of the sensor channel centered at λ_i. Since there is no post-launch information on the random noise in the SeaWiFS measurements (R.A. Barnes, personal communication), pre-launch NE$\Delta L(\lambda_i)$ values were used (Barnes et al., 1994). For MODIS (Terra) NE$\Delta L(\lambda_i)$ were taken from Barnes et al. (2003). $E(\lambda_i)$ was computed using the atmospheric radiative code 6S (Vermote et al., 1997) for
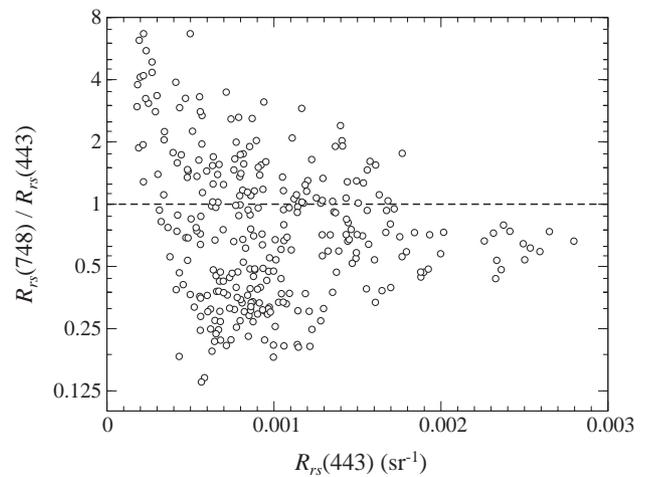

Fig. 3. Ratio of near-infrared to blue R_{rs} as a function of R_{rs} in the blue spectral region.
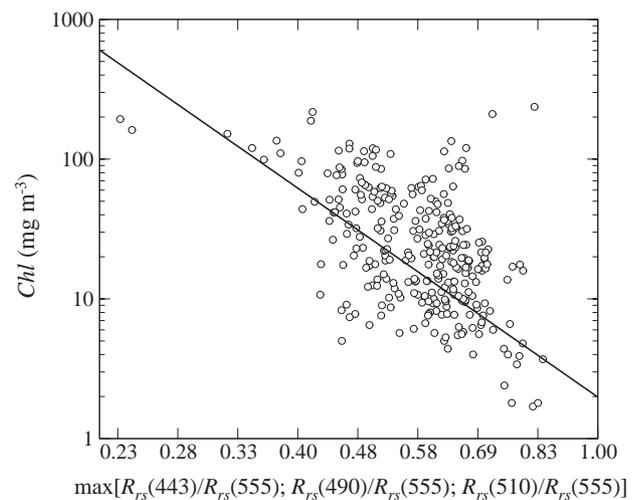

Fig. 2. Normalized frequency distribution of the Chl data that were used in this study.

Fig. 4. Relationship between observed Chl and max[R_{rs}(443)/R_{rs}(555); R_{rs}(490)/R_{rs}(555); R_{rs}(510)/R_{rs}(555)] (circles). The solid line shows the Chl values predicted by the SeaWiFS OC4V4 algorithm.

a Mid-latitude Summer atmosphere worst case scenario: the solar zenith angle and the aerosol optical thickness at 550 nm (aot550) were set a 60° and 0.44, respectively. The resulting $NE\Delta R_{rs}(\lambda_i)$ are reported in Table 2.

Eq. (3) was evaluated at four Chl values: 10, 20, 50 and 100 mg m^{-3}. To calculate typical $R_{rs}(\lambda_i)$ values corresponding to these Chl, we selected from the calibration subset stations with Chl ranging within ±15% of the above four

selected Chl values. The median values of Chl and $R_{rs}(\lambda_i)$ were then computed for each of the Chl (Table 3). Note that while $R_{rs}(NIR)$ increased with increasing Chl due to the concurrent increase in the backscattering coefficient, $R_{rs}(red)$ appeared to be weakly correlated with Chl due to a compensation between the increase in absorption and backscattering coefficients (Gitelson et al., 1999). Using these median values the overall relative random uncertainty
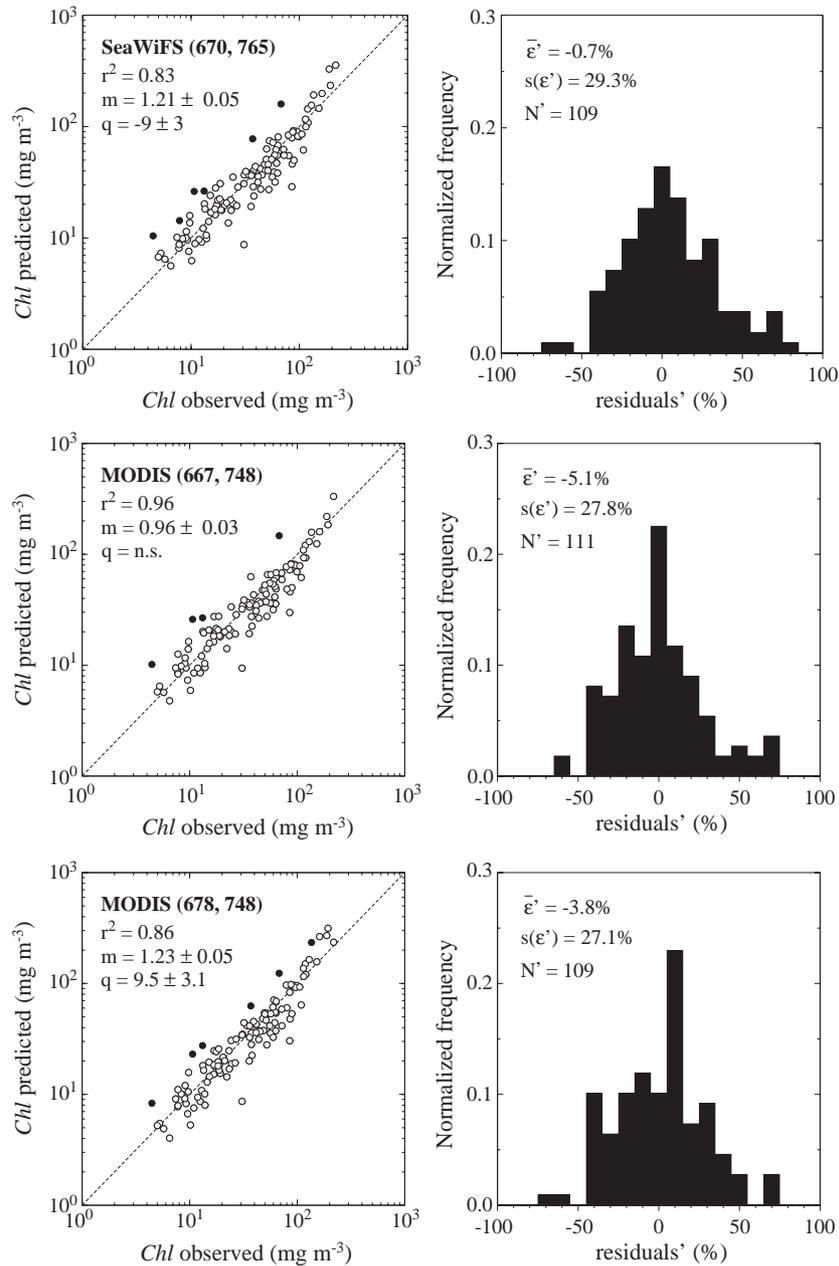

Fig. 5. Validation results for the algorithms SeaWiFS(670,765), MODIS(667,748) and MODIS(678,748). Left column: scatter plots between observed and predicted Chl along with the slope, m, and intercept, q, (±their standard errors) and determination coefficient (r^2) of the linear fit Chl_{pred} vs. Chl_{obs}. The intercept and slope of MODIS(667,748) were not significantly different from zero and one, respectively ($p > 0.05$). Right column: normalized frequency distribution of the percent residuals ε'_i; $\overline{\varepsilon}'$ is the average of ε'_i and it is used as an estimate of the average bias; $s(\varepsilon')$ is the experimental standard deviation of ε'_i and it is used as an estimate of the typical random uncertainty associated with a prediction of Chl; N' is the number of samples. The prime indicates that the quantities were calculated after removing outliers for which $\varepsilon_i > 2s(\varepsilon)$ (full black circles). The initial number of samples was 115.

in *Chl* estimation was computed from Eq. (2) as a function of g_r for each model presented in Table 1.

Finally, the uncertainty budget for each algorithm was calculated for $g_r = 5$. More precisely, the terms composing the right hand side of Eq. (3) were evaluated separately for each band, for both the uncorrelated part of the *Chl* noise arising from R_{rs} random uncertainties (i.e. $Chl^{-1} \times \{[\partial Chl / \partial R_{rs}(\lambda_i)]^2 \times s^2[R_{rs}(\lambda_i)]_{sens}\}^{0.5}$), and for its correlated part (i.e. $Chl^{-1} \times \{|\partial Chl / \partial R_{rs}(\lambda_i) \times \partial Chl / \partial R_{rs}(\lambda_j) \times s^2[R_{rs}(\lambda_i)]_{sens} \times r(\lambda_i, \lambda_j)|\}^{0.5}$, where the absolute value is needed because the argument inside curly parentheses can be negative). By taking the square root of the sum of squares of these terms, as well as of the noise generated by the bio-optical algorithm, one obtains the overall relative random uncertainty in *Chl* estimation.

2.7. Systematic errors

Systematic errors are deviations from the true value of a measured quantity (R_{rs} and *Chl* in our case) that cannot be reduced by averaging a large number of measurements (BIPM & ISO, 1995). The accuracy of the measurement is therefore affected by these types of errors as they introduce a bias in the measured quantity. Such uncertainties can arise in R_{rs} measurements for example from offsets in the calibration coefficients of the radiometer or from an imperfect atmospheric correction scheme. An analysis of the effects of R_{rs} systematic errors on the predicted *Chl* was carried out for the MODIS(667, 748) algorithm and for the R_{rs} values corresponding to approximately 20 mg m^{-3} (Table 3). The magnitude of the $R_{rs}(\lambda)$ systematic error was defined as a fraction $g_s(\lambda)$ of the reflectance measured in the 748 nm MODIS band at *Chl* = 20 mg m^{-3}:

$$\varepsilon(\lambda) = g_s(\lambda) R_{rs}(748) \qquad (7)$$

where λ is the central wavelength of the band under exam.

$g_s(667)$ and $g_s(748)$ were varied between -1 and $+1$ and the resulting $\varepsilon(\lambda)$ were added to the corresponding values of $R_{rs}(\lambda)$. Finally, the relative change in the predicted *Chl* was computed as $\Delta Chl / Chl = (Chl_\varepsilon - Chl_0)/Chl_0$, where Chl_ε is the *Chl* predicted by the band ratio

$[R_{rs}(748) + \varepsilon(748)]/[R_{rs}(667) + \varepsilon(667)]$ using the relationships presented in Table 4; Chl_0 is the *Chl* predicted in the absence of $\varepsilon(\lambda)$ errors.

3. Results

The lakes sampled were characterized by high variability in *Chl*, turbidity and Secchi disk depth (Table 5 and Fig. 2). Average values of TSS, $a_{CDOM}(440)$ and $a_{det}(440)$ were high and typical of inland turbid productive waters. Remote-sensing reflectance spectra were also characteristics of such waters (e.g. Gons et al., 2000) and displayed local maxima around 560 and 700 nm (Fig. 1). Due to the high total absorption coefficient in the blue spectral region, as well as to the high total backscattering coefficient, R_{rs}(NIR) was higher than R_{rs} around 440 nm about 40% of the times (Fig. 3).

Fig. 4 demonstrates that algorithms based on reflectances in the blue-green spectral region, as the OC4V4 SeaWiFS (O'Reilly et al., 1998), are not suitable for estimating *Chl* in turbid productive waters. While the OC4V4 algorithm followed the trend of the data, the average random deviation was approximately 88%, in accord with the results presented by Darecki and Stramski (2004) for the Baltic Sea.

The results of the validation, obtained using the independent subset of data are presented in Fig. 5 and Table 6. NIR-to-red reflectance ratios applied to SeaWiFS and MODIS channels predicted *Chl* with an average underestimation of about 3% and with a typical uncertainty in *Chl* prediction of about 28%. Between the two algorithms tested for MODIS, the MODIS(667,748) appeared to provide the most accurate prediction of *Chl*: the slope and intercept of the 1:1 line were not significantly different from one and zero, respectively ($p > 0.05$). No clear pattern was found to explain the outliers excluded from the validation (filled black circles in Fig. 5); they may be related to uncertainties in the measurements of both R_{rs} and *Chl*.

The overall random *Chl* uncertainties are presented in Fig. 6 as a function of the random uncertainties in R_{rs}. For a fixed g_r, $[s(Chl)/Chl]_{system}$ was inversely related to *Chl* and it was lower for positively correlated atmospheric uncer-

Table 6
Results of the validation of the proposed algorithms

Algorithm	m (se)	q (se) (mg m^{-3})	r^2	$s(\varepsilon)$ (%)	$\overline{\varepsilon'}$ (%)	$s(\varepsilon')$ (%)	RMSE' (mg m^{-3})	N'
SeaWiFS(670, 765)	1.21 (0.05)	−9 (3)	0.83	39.3	−0.7	29.3	24.4	109
MODIS(667, 748)	**0.96** (0.03)	–	0.84	36.1	−5.1	27.8	18.1	111
MODIS(678, 748)	1.23 (0.05)	−9.5 (3.1)	0.86	33.8	−3.8	27.1	21.8	109

For each algorithm the following statistics are reported: the slope (m; in bold those not significantly different from one, $p > 0.01$) and intercept (q) of the Chl_{Pred} vs. Chl_{Obs} line with their standard errors (se), the coefficient of determination, the experimental standard deviation [$s(\varepsilon)$] of the relative residuals ε_i, the average ($\overline{\varepsilon'}$) and experimental standard deviation [$s(\varepsilon')$] of ε_i', the root mean squared error (RMSE') and the number of samples (N'). The prime indicates that the quantities were calculated after removing stations for which $\varepsilon_i > 2s(\varepsilon)$. The number of samples before the removal of outliers was 115.
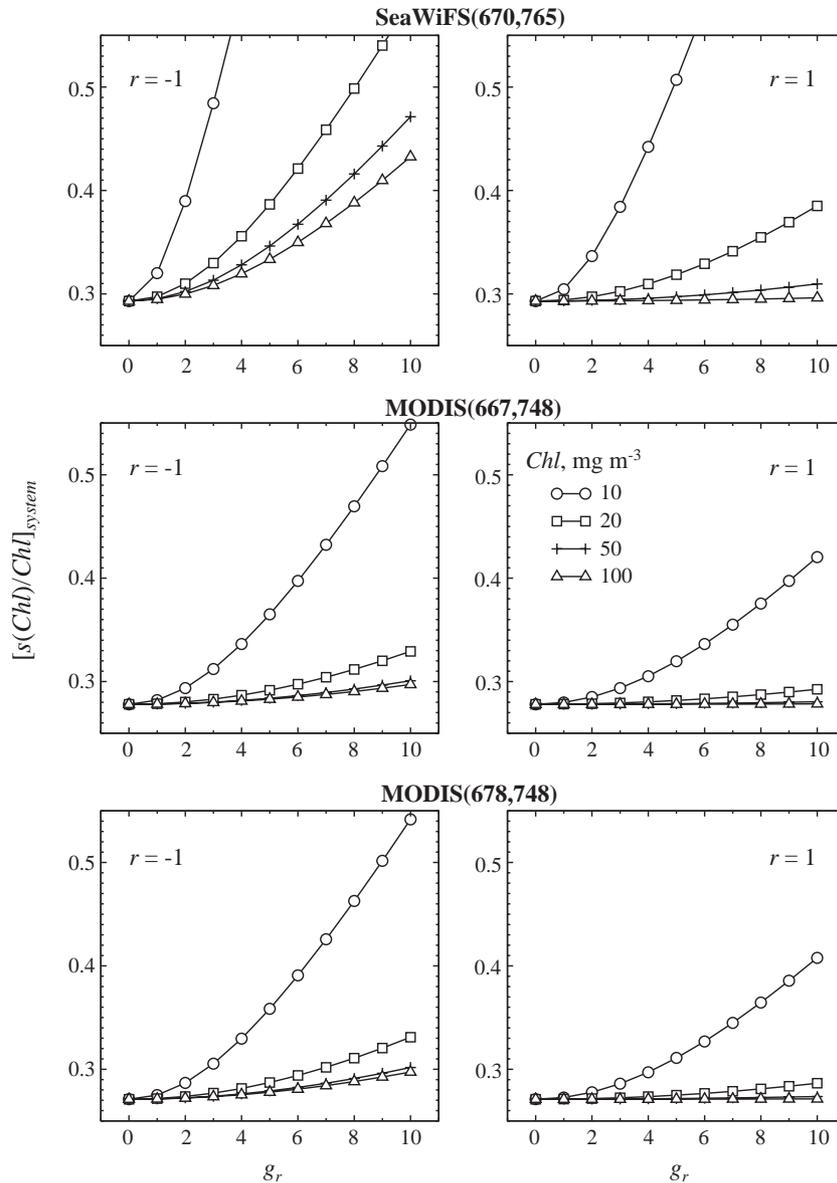
Fig. 6. Overall relative random *Chl* uncertainties for selected values of *Chl* (indicated with different symbols) as a function of the random R_{rs} uncertainty (g_r). R_{rs} uncertainties are negatively correlated ($r = -1$) in the left column and positively correlated ($r = 1$) in the right column. $g_r \times NE\Delta R_{rs}$ (NIR) provides the absolute magnitude of the R_{rs} random uncertainty used. The value of $[s(Chl)/Chl]_{system}$ for $g_r = 0$ indicates the random uncertainty in *Chl* due only to the NIR-to-red reflectance ratio.

tainties ($r = 1$). The three algorithms were affected by comparable overall *Chl* uncertainties: in the worst case scenario ($r = -1$), MODIS could estimate $Chl \geq 10$ mg m^{-3} with a random uncertainty lower than 40%, provided the R_{rs} random uncertainties were about 6 times the NEΔR_{rs}(748). A difference between SeaWiFS and MODIS algorithms was evident at $Chl = 10$ mg m^{-3}: $[s(Chl)/Chl]_{system}$ was considerably higher for SeaWiFS than for MODIS due to the lower radiometric sensitivity of SeaWiFS (Table 2).

Tables 7, 8 and 9 present the uncertainty budgets for each algorithm in the case $g_r = 5$. Similar qualitative behaviors were found among the three algorithms. The major contributor to the overall *Chl* uncertainty was the bio-

optical algorithm itself. Moreover, of the two bands used in the algorithm, the NIR band accounted for the majority of the *Chl* uncertainty, but its contribution decreased and became progressively more comparable to that of the red band as *Chl* increased. As a consequence, also the magnitude of the overall *Chl* uncertainty was inversely related to *Chl*. Finally, as *Chl* increased, the absolute value of the correlation factor progressively decreased and, in the case of positively correlated R_{rs} uncertainties, the overall *Chl* uncertainty at $Chl = 10^3$ mg m^{-3} was practically independent of the R_{rs} random uncertainty.

Fig. 7 shows the relative biases in the predicted *Chl* due to R_{rs} systematic errors. As for random uncertainties, R_{rs}

Table 7
SeaWiFS(670, 765) uncertainty budget for $g_r=5$ and different *Chl* levels

Chl (mg m^{-3})	$\left[\frac{s(Chl)}{Chl}\right]_{bio}$	$\left[\frac{s(Chl)}{Chl}\right]_{sens}$			$\left[\frac{s(Chl)}{Chl}\right]_{system}$		
		Red	NIR	Correl. fact.	$r=-1$	$r=0$	$r=1$
9.9	0.293	0.115	0.528	0.348	0.707	0.615	0.507
19.6	0.293	0.064	0.189	0.155	0.387	0.354	0.319
45.9	0.293	0.067	0.117	0.126	0.346	0.323	0.297
103.5	0.293	0.069	0.090	0.112	0.333	0.314	0.294

The contribution of each term composing $[s(Chl)/Chl]_{system}$ is presented. The contribution of each sensor band to $[s(Chl)/Chl]_{sens}$ and the absolute value of the correlation factor (see Eq. (3)) are also reported. Note that the correlation factor was always positive when $r=-1$, and always negative when $r=1$. The quadrature sum of each term in a row (including the correlation factor with the appropriate sign, when necessary) gives the estimated $[s(Chl)/Chl]_{system}$ for the selected *Chl* range.

systematic errors in the NIR band were, in general, responsible for larger biases in *Chl* than those associated to the red channel. For example, $|\Delta Chl/Chl|$ for $g_s(667)=+0.2$ and $g_s(748)=0$ is less than 1/3 than for $g_s(667)=0$ and $g_s(748)=+0.2$. The worst case scenarios corresponded to R_{rs} systematic errors of opposite signs, especially for positive and negative deviations in $R_{rs}(748)$ and $R_{rs}(667)$, respectively. In contrast, minimal *Chl* biases were obtained when deviations in R_{rs} had the same signs and, generally, the relative *Chl* biases could be kept lower than $\pm35\%$ provided $g_s(748)\leq\pm10\%$ and $-35\%\leq g_s(748)\leq+50\%$. For other *Chl* values, qualitatively similar results were obtained (not shown). Finally, these calculations do not depend on the radiometric sensitivity of the sensor, but only on the form of the algorithm used (which was consistent for SeaWiFS and MODIS); thus, quantitatively similar results (not shown) were obtained when this

Table 8
As Table 7 for MODIS(667,748)

Chl (mg m^{-3})	$\left[\frac{s(Chl)}{Chl}\right]_{alg}$	$\left[\frac{s(Chl)}{Chl}\right]_{sens}$			$\left[\frac{s(Chl)}{Chl}\right]_{system}$		
		Red	NIR	Correl. fact.	$r=-1$	$r=0$	$r=1$
9.9	0.278	0.039	0.197	0.125	0.365	0.343	0.320
19.6	0.278	0.021	0.067	0.053	0.292	0.287	0.282
45.9	0.278	0.020	0.038	0.039	0.284	0.281	0.279
103.5	0.278	0.023	0.030	0.037	0.283	0.281	0.278

Table 9
As Table 7 for MODIS(678,748)

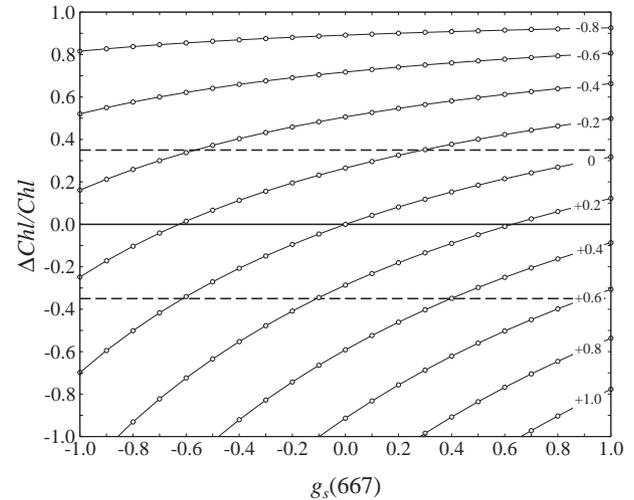| Chl (mg m^{-3})	$\left[\frac{s(Chl)}{Chl}\right]_{alg}$	$\left[\frac{s(Chl)}{Chl}\right]_{sens}$			$\left[\frac{s(Chl)}{Chl}\right]_{system}$		
		Red	NIR	Correl. fact.	$r=-1$	$r=0$	$r=1$
9.9	0.271	0.041	0.194	0.126	0.358	0.336	0.311
19.6	0.271	0.024	0.071	0.059	0.287	0.281	0.275
45.9	0.271	0.024	0.043	0.045	0.279	0.275	0.272
103.5	0.271	0.027	0.034	0.043	0.278	0.275	0.271

Fig. 7. *Chl* relative biases as a function of R_{rs} systematic uncertainties for the MODIS(667,748) algorithm when estimating $Chl=20$ mg m^{-3}. Numbers inside the graph indicate values of $g_s(748)$. $g_s(\lambda)\times R_{rs}$ (748) provides the absolute magnitude of the systematic uncertainty of R_{rs} (λ). Dashed lines represent a potential $\pm35\%$ goal in *Chl* accuracy.

analysis was applied to the algorithms SeaWiFS(670,765) and MODIS(675,748).

4. Discussion and conclusions

The purpose of this study was to evaluate the extent to which NIR-to-red reflectance ratios can be applied to SeaWiFS and MODIS data to estimate *Chl* in productive turbid waters. To achieve this objective, first, using hyperspectral R_{rs} data collected in situ over a wide range of optical constituents (Table 2), we calibrated and validated *Chl* algorithms using simulated SeaWiFS and MODIS red and NIR bands. The data used in this study were collected in inland waters, but encompassed *Chl* values that are commonly found in coastal and estuarine waters. For example, from *Chl* data on the Chesapeake Bay (Harding & Perry, 1997) it appears that from 1950 to 1994 there was approximately a 50% probability of finding *Chl* values larger than 10 mg m^{-3}. Moreover $Chl\geq10$ mg m^{-3}, and as high as 100 mg m^{-3}, have been reported for European coastal waters as well (e.g. Babin et al., 2003; Darecki & Stramski, 2004). Thus, we believe that the presented algorithms could be also applied to SeaWiFS and MODIS data collected in coastal turbid waters.

Second, we assessed the extent to which the proposed algorithms would be affected by random uncertainties in R_{rs}. Because at present there is no operational atmospheric correction for the red and NIR bands of SeaWiFS and MODIS, we expressed the R_{rs} random uncertainties due to the sensor radiometric noise as a proportion of NEΔR_{rs} (NIR). It was found that, for a worst case atmospheric scenario (i.e. negatively correlated atmospheric uncertainties, solar zenith angle $=60°$, aot550 $=0.44$), MODIS should

be able to estimate $Chl \geq 10$ mg m^{-3} with an overall random uncertainty <40%, provided that R_{rs} random uncertainties are 6 times the NEΔR_{rs}(748). Lower solar zenith angles, smaller aot550 and positively correlated R_{rs} uncertainties should allow more precise estimates of Chl (for R_{rs} uncertainties of the same magnitude). Moreover, the lower radiometric sensitivity of SeaWiFS caused larger uncertainties in the predicted Chl especially at low Chl values. This implies that it may not be possible to use the proposed SeaWiFS algorithm for estimating Chl lower than approximately 15 mg m^{-3} with a precision of 40%.

The uncertainty budgets allowed us to identify the major contributors to the overall random Chl uncertainty: i.e. a) the uncertainty due to the bio-optical algorithm, and b) the R_{rs} random uncertainty in the NIR band (Tables 7–9). While the former is intrinsic in the algorithms adopted in this study and larger than those obtained in case-1 waters (e.g. O'Reilly et al., 1998), the latter can be related to the sensitivity of the algorithm (I) with respect to $R_{rs}(\lambda_i)$, i.e. $\partial I / \partial R_{rs}(\lambda_i)$. Indeed, for $Chl < 100$ mg m^{-3}, $\partial I / \partial R_{rs}$(NIR) is higher than $\partial I / \partial R_{rs}$(red) (not shown), i.e. the value of I changes more for a change in R_{rs}(NIR) than for a change in R_{rs}(red). This explains why the NIR band is the greatest contributor to $[s(Chl)/Chl]_{system}$. Moreover as Chl increases, $\partial I / \partial R_{rs}$(NIR) decreases more steeply than $\partial I / \partial R_{rs}$(red); thus, the contributions of the two bands to the overall random Chl uncertainty become progressively comparable at high Chl values.

Finally, the effects of R_{rs} systematic errors on the predicted Chl were studied. It was found that the accuracy of Chl was mostly dependent on systematic errors in R_{rs}(NIR). In the best case scenario, i.e. R_{rs}(NIR) underestimated by 20% and R_{rs}(red) underestimated by approximately 30%, the band ratios were robust and could predict Chl with a bias lower than ±35%. Remarkably, $|\Delta Chl / Chl|$ was lower than 35% even for very larger errors (e.g. $g_s(748) = -0.4$ and $g_s(667) = -0.9$) provided they had similar signs and that $|g_s(748)| < |g_s(667)|$. Therefore, since correlated systematic errors are typical of imperfect atmospheric correction schemes (Ruddick et al., 2001), the presented band ratios might be also robust with respect to imperfect atmospheric corrections.

The atmospheric correction requirements presented above can be compared to those computed for the case-1 water atmospheric correction procedure of the blue-green MODIS bands. Gordon and Voss (1999) estimated that, for the MODIS band centered at 443 nm, the required (systematic) uncertainty due atmospheric correction should be between five to ten times the NEΔR_{rs} of the same channel. From this study it appears that, to have a Chl bias smaller than ±35%, the R_{rs}(NIR) systematic uncertainty should be about 8 times the NEΔR_{rs}(NIR) in the case of SeaWiFS and about 24 times in the case of MODIS. This difference is due to the lower signal-to-noise ratio of SeaWiFS. The R_{rs} uncertainty requirements in case-1 water are of 5% for the bands in the visible spectral range (Gordon

& Voss, 1999). Thus, we believe that over turbid productive waters, an uncertainty in R_{rs}(NIR) of ±20% (at $Chl = 20$ mg m^{-3}), is a realistic (if not conservative) estimate of the R_{rs} systematic uncertainty.

The proposed methodology is likely applicable for the estimation of Chl in other water bodies. Specifically, we expect the calibration coefficients presented to be robust with regard to variations in total absorption and backscattering coefficients, provided that these variations are within the wide range sampled in this study (Table 5). However, it is worth describing how the natural variability of a and b_b could affect the proposed algorithm. Variations in the phytoplankton specific absorption coefficient, a_ϕ^*, would cause changes in the estimated Chl. More precisely, sensitivity studies (not shown) suggest that, for Chl ranging from 10 to 100 mg m^{-3}, variations in a_ϕ^*(red) by ±50% would determine a change in the estimated Chl ranging approximately from ±25% to ±60%, respectively. On the other hand, the backscattering coefficient of phytoplankton, $b_{b\phi}$ is, in general, spectrally dependent, but its contribution to the total backscattering coefficient is negligible so that b_b does not show prominent spectral features (e.g. Ahn et al., 1992). This is especially true when mineral particles are present in suspension, as in turbid coastal waters. However, there may be occasions, such as in the case of a phytoplankton bloom, in which b_b may be comparable to $b_{b\phi}$ and thus it may show spectral features such as a local minimum in correspondence with the red absorption maximum of chlorophyll-a. In such cases one would expect the proposed algorithms to overestimate Chl.

Variations in the optical properties of non-algal suspended particles as well as CDOM could affect the algorithm as follows. High loadings of non-algal particles may cause a significant absorption in the red and NIR spectral regions (e.g. Tassan & Ferrari, 1995). In such circumstances one of the hypotheses upon which the algorithm is based breaks down and an overestimation of Chl is expected. However, such overestimation would be reduced by the reflectance ratio. Finally, the backscattering coefficient of non-algal suspended particles may vary linearly with wavelength (instead of being spectrally flat as assumed). In such cases, one should expect an underestimation or overestimation of Chl, for a negative or positive λ-dependence of b_b, respectively.

The uncertainty estimates presented in Table 6 account for all the types of variations in optical properties discussed above and average to approximately 28%. Therefore we believe that the proposed algorithms are robust for estimating Chl in turbid productive waters. More validation is nonetheless needed for water bodies with different optical characteristics.

In conclusion, this study suggests that SeaWiFS and MODIS have the potential to estimate Chl in turbid productive waters exploiting NIR-to-red reflectance ratios. This is because, in such waters, the signal upwelling in the red and NIR spectral regions carries precious information

about the phytoplankton absorption and total backscattering coefficients. Our findings imply that the existing data archive of SeaWiFS and MODIS (from both Terra and Aqua spacecrafts) images could be used to study quantitatively the dynamics of turbid productive water ecosystems. The main obstacle to this achievement is the lack of an operational atmospheric correction scheme over turbid waters specific for the red and NIR bands.

Acknowledgements

References

Ahn, Y., Bricaud, A., & Morel, A. (1992). Light backscattering efficiency and related properties of some. *Deep-Sea Research. Part A, Oceanographic Research Papers*, *38*(11–12A), 1835–1855.

American Public Health Association, American Water Works Association, & Water Pollution Control Federation. (1989). *Standard methods for the examination of water and wastewater*. Washington, D.C.: American Public Health Association.

Babin, M., Stramski, D., Ferrari, G. M., Claustre, H., Bricaud, A., Obolensky, G., et al. (2003). Variations in the light absorption coefficients of phytoplankton, nonalgal particles, and dissolved organic matter in coastal waters around Europe. *Journal of Geophysical Research—Oceans*, *108*(C7), 3211.

Barnes, R. A., Barnes, W. L., Esaias, W. E., & McClain, C. R. (1994), SeaWiFS prelaunch technical report series volume 22, Prelaunch Acceptance Report for the SeaWiFS Radiometer. NASA, *Technical Memorandum— SeaWIFS Prelaunch Technical Report Series no.22*, 1–35.

Barnes, W., Xiong, X., & Salomonson, V. (2003). Status of Terra MODIS and Aqua MODIS. *Advances in Space Research*, *32*(11), 2099–2106.

BIPM, & ISO. (1995). *Guide to the expression of uncertainty in measurement*. Geneve, Switzerland: International Organization for Standardization, p. 101.

Carder, K. L., Chen, F. R., Lee, Z. P., Hawes, S. K., & Kamykowski, D. (1999). Semianalytic moderate-resolution imaging spectrometer algorithms for chlorophyll a and absorption with bio-optical domains based on nitrate-depletion temperatures. *Journal of Geophysical Research—Oceans*, *104*(C3), 5403–5421.

Dall'Olmo, G., & Gitelson, A. A. (2005). Effect of bio-optical parameter variability on the remote estimation of chlorophyll-a concentration in turbid productive waters: Experimental results. *Applied Optics*, *44*(3), 412–422.

Dall'Olmo, G., Gitelson, A. A., & Rundquist, D. C. (2003). Towards a unified approach for remote estimation of chlorophyll-a in both terrestrial vegetation and turbid productive waters. *Geophysical Research Letters*, *30*(18), 1938.

Darecki, M., & Stramski, D. (2004). An evaluation of MODIS and SeaWiFS bio-optical algorithms in the Baltic Sea. *Remote Sensing of Environment*, *89*(3), 326–350.

Dekker, A. G. (1993). Detection of optical water quality parameters for eutrophic waters by high resolution remote sensing. *Ph.D. Thesis*, Vrije Universiteit, Amsterdam, p. 222.

Garver, S. A., & Siegel, D. A. (1997). Inherent optical property inversion of ocean color spectra and its biogeochemical interpretation: 1. Time series from the Sargasso Sea. *Journal of Geophysical Research—Oceans*, *102*(C8), 18607–18625.

Gitelson, A. A., & Kondratyev, K. Y. (1991). Optical models of mesotrophic and eutrophic water bodies. *International Journal of Remote Sensing*, *12*(3), 373–385.

Gitelson, A. A., Schalles, J. F., Rundquist, D. C., Schiebe, F. R., & Yacobi, Y. Z. (1999). Comparative reflectance properties of algal cultures with manipulated densities. *Journal of Applied Phycology*, *11*, 345–354.

Gons, H. J. (1999). Optical teledetection of chlorophyll a in turbid inland waters. *Environmental Science and Technology*, *33*(7), 1127–1132.

Gons, H. J., Rijkeboer, M., Bagheri, S., & Ruddick, K. G. (2000). Optical teledetection of chlorophyll a in estuarine and coastal waters. *Environmental Science and Technology*, *34*(24), 5189–5192.

Gons, H. J., Rijkeboer, M., & Ruddick, K. G. (2002). A chlorophyll-retrieval algorithm for satellite imagery (Medium Resolution Imaging Spectrometer) of inland and coastal waters. *Journal of Plankton Research*, *24*(9), 947–951.

Gordon, H. R. (1990). Radiometric considerations for ocean color remote sensors. *Applied Optics*, *29*(22), 3228–3236.

Gordon, H. R., & Voss, K. J. (1996). *MODIS normalized water-leaving radiance Algorithm Theoretical Basis Document (MOD 18). Version 4*. http://modis.gsfc.nasa.gov/data/atbd/atbd_mod17.pdf, Accessed on December 17th, 2004.

Gordon, H. R., & Wang, M. H. (1994). Retrieval of water-leaving radiance and aerosol optical thickness over the oceans with SeaWiFS: A preliminary algorithm. *Applied Optics*, *33*(3), 443–452.

Harding, L. W., & Perry, E. S. (1997). Long-term increase of phytoplankton biomass in Chesapeake Bay, 1950–1994. *Marine Ecology. Progress Series*, *157*, 39–52.

Hoge, F. E., & Lyon, P. E. (1996). Satellite retrieval of inherent optical properties by linear matrix inversion of oceanic radiance models: An analysis of model and radiance measurement errors. *Journal of Geophysical Research—Oceans*, *101*(C7), 16631–16648.

IOCCG Report Number 1. (1998). *Minimum requirements for an operational ocean-colour sensor for the open ocean*. Canada: Dartmouth, p.46.

Lee, Z. P., Carder, K. L., Hawes, S. K., Steward, R. G., Peacock, T. G., & Davis, C. O. (1994). Model for the interpretation of hyperspectral remote-sensing reflectance. *Applied Optics*, *33*(24), 5721–5732.

Lyon, P., Hoge, F., Wright, C., Swift, R., & Yungel, J. (2004). Chlorophyll biomass in the global oceans: Satellite retrieval using inherent optical properties. *Applied Optics*, *43*(31), 5886–5892.

Ohde, T., & Siegel, H. (2003). Derivation of immersion factors for the hyperspectral Trios radiance sensor. *Journal of Optics. A, Pure and Applied Optics*, *5*(3), 12–14.

O'Reilly, J. E., Carder, K. L., Garver, S. A., Kahru, M., McClain, C., Maritorena, S., et al. (1998). Ocean color chlorophyll algorithms for SeaWiFS. *Journal of Geophysical Research C: Oceans*, *103*(C11), 24937–24953.

Quan, X., & Fry, E. (1995). Empirical-equation for the index of refraction of seawater. *Applied Optics*, *34*(18), 3477–3480.

Ruddick, K. G., Gons, H. J., Rijkeboer, M., & Tilstone, G. (2001). Optical remote sensing of chlorophyll a in case 2 waters by use of an adaptive two-band algorithm with optimal error properties. *Applied Optics*, *40*(21), 3575–3585.

Ruddick, K. G., Ovidio, F., & Rijkeboer, M. (2000). Atmospheric correction of SeaWiFS imagery for turbid coastal and inland waters. *Applied Optics*, *39*(6), 897–912.

Sandmeier, S., Müller, C., Hosgood, B., & Andreoli, G. (1998). Sensitivity analysis and quality assessment of laboratory BRDF data. *Remote Sensing of Environment*, *64*, 176–191.

Schiller, H., & Doerffer, R. (1999). Neural network for emulation of an inverse model—Operational derivation of case II water properties from MERIS data. *International Journal of Remote Sensing*, *20*(9), 1735–1746.

Tassan, S., & Ferrari, G. M. (1995). An alternative approach to absorption measurements of aquatic particles retained on filters. *Limnology and Oceanography*, *40*(8), 1358–1368.

Vermote, E. F., Tanre, D., Deuze, J. L., Herman, M., & Morcrette, J. J. (1997). Second simulation of the satellite signal in the solar spectrum, 6s: An overview. *IEEE Transactions on Geoscience and Remote Sensing*, *35*(3), 675–686.

Welschmeyer, N. A. (1994). Fluorometric analysis of chlorophyll a in the presence of chlorophyll b and pheopigments. *Limnology and Oceanography, 39*(8), 1985–1992.

Yacobi, Y. Z., Gitelson, A. A., & Mayo, M. (1995). Remote sensing of chlorophyll in Lake Kinneret using high-spectral-resolution radiometer and Landsat TM: Spectral features of reflectance and algorithm development. *Journal of Plankton Research*, *17*(11), 2155–2173.

Zibordi, G., Melin, F., Hooker, S. B., D'alimonte, D., & Holbert, B. (2004). An autonomous above-water system for the validation of ocean color radiance data. *IEEE Transactions on Geoscience and Remote Sensing*, *42*(2), 401–415.